International Journal of Computer Information Systems and Industrial Management Applications
ISSN 2150-7988 Volume 18(2s) 2026 pp. 1021-1038
https://doi.org/10.70917/ijcisim-2026-2186
Article

# IMAGE ENHANCEMENT THROUGH EDGE PRESERVATION: A MULTI-LEVEL HYBRID DENOISING, RIDGELET AND CURVELET BASED TECHNIQUE

**Khakon Das[1,3]*, Ashish Khare[1], Nilesh Anand Srivastava[1], Manish Khare[2], Ranjan Kumar Mondal[3]**

[1]Department of Electronics & Communication, University of Allahabad, Prayagraj – 211002, India, ashishkhare@allduniv.ac.in; nilesh@allduniv.ac.in
[2]Department of Computer Science, Allahabad Degree College, Prayagraj – 211002, India, mkharejk@gmail.com
[3]Department of Computer Science and Engineering, Swami Vivekananda University, Kolkata – 700121, India, khakon.phd2021@allduniv.ac.in; ranjankm@svu.ac.in
**Corresponding Author:** Khakon Das (Email: (khakon.phd2021@allduniv.ac.in)

**Abstract:** Medical image is one of the post power full tools for studying neurological disorders. Epilepsy is one of the them. Over 50 millions peoples are suffered from epilepsy. Medical image can used to study the epilepsy, as the brain stroke, brain tumor, and brain injuries are the most common causes of it. Here image pre-processing plays a significance role to enhance the quality of the input image. Further, image registration, noise removal, image enhancement, etc. are the common processes involved in pre-processing. An Efficient real time embedded solution for medical image enhancement is needed. In the area of machine learning (ML) and artificial intelligent (AI) solution, most of existing algorithms are software based and their hardware implementation is difficult. However, hardware implementation of such algorithm is needed for real time performance. This work proposes a image enhancement technique based on wavelet, Ridgelet and curvelet transform. Here a modified Haar wavelet transform with sliding window-based overlapping execution is use for image denoising with a dedicated embedded hardware implementation. The proposed algorithm provides a solution for image enhancement by image's edge preservation. Further the image edges have been preserved by Ridgelet and modified curvelet transform based technique. Performance of the projected image enhancement algorithm has been evaluated in terms of many statistics approached namely peak signal-to-noise ratio (PSNR), mean square error (MSE), mutual information (MI), universal image quality index (UIQI), geometric mean (Gm), and gradient (Gd). The results obtained by applying the projected algorithm demonstrate the significant improvement in output image quality. Further, the embedded version of the proposed algorithm has been successfully implemented into ESP32-WiFi Cam module powered by tiny 32-bits processor architecture, small amount of primary memory along with dedicated SD card slot for storage. Further it has been observed that the in-place calculation with software pipelining technique offers memory and time efficient solution. Further, lower computational overhead results in fewer resource requirements which make the proposed solution suitable for real time and portable...

**Keywords**: Curvelet, Edge Preservation, Embedded System, Image Enhancement, Multi Level Denoising, Ridgelet, Wavelet

## 1. INTRODUCTION

In image enhancement enhance the image quality without altering the basic image characteristics. Specifically, in medical science, image enhancement plays important roles to achieve clinically acceptable images. For this, various image enhancement techniques have already been suggested in recent literature [1-8]. The techniques like image denoising [1, 2], image contrast enhancement [3, 4], edge preservation [5], and fusion of multi-modal images [6-8]

have been proposed to secure the image information in terms of edge, curve etc. In the below subsection a detailed literature survey about medical image quality enhancement has been perform.

## 2. BACKGROUND

Earlier, Mallat et al. [9] had introduced a discrete wavelet transform (DWT) model for the effective denoising of medical images [10, 11] and further various suggestions has also been made to modify DWT. Further, Sweldens & Daubechies proposed a novel concept named as lifting scheme [12, 13], that in-turn offers the design and execution of wavelet transform simultaneously [14, 15]. Due to its straightforward arithmetic calculations and wide uses in medical image processing, Haar wavelet transform (HWT) has been used in numerous state-of-the-arts [16-18]. As, Das et al. [10] used a fusion method for the denoising of individual as well fused medical images using modified Haar wavelet transform (MHWT). In [19] an adaptive denoising technique used to enhance the visual quality of computed tomography (CT) images. In recommended idea fuses the images denoised by total variation (TV), curvelet method techniques. The edge information is collected from the noise residue output of TV method through use of curvelet transform. This successfully reduces the staircase effect and visual distortion from the given images and produced enhanced image [19]. Further approximate digital implementation of some mathematical transforms, namely, the curvelet, Ridgelet, wavelet, and radon transform [20, 21] has been implemented in [22]. This approach offers an accurate reconstruction, stability against perturbations, and low computational complexity in ease of implementation. Here a very simple interpolation in Fourier space is use, which takes yields samples and Cartesian samples on a recto polar grid. It represents a pseudo-polar sampling set based on concentric squares geometry. Further a Ridgelet transform applies with the radon transform, a special over complete wavelet. Where Ridgelet and curvelet transform with filter bank approach is used to enhance the given image. Moreover, the curvelet based image reconstructions put on display the higher perceptual quality of images than wavelet-based reconstructions. It produced visually sharper images, by the higher quality recovery of edges, weak lines and curvilinear features [22].

From the above study it is clear that a Ridgelet and curvelet transform based image enhancement methods are more efficient than only wavelet-based image enhancement method. The hardware level implementation of those techniques can make them more efficient. Here the speed improvements achieved through FPGA implementation by the used of real-time clock frequency and improve the space efficiency using available resources of FPGA Board [23, 24, 25]. In [26], a pipeline-based FPGA design for the hardware implementation of discrete wavelets transforms (db2, db4, and db8) using high-pass and low-pass filters has been provided. This design utilizes 506 logic elements, a 3200-bit RAM [26]. Next, Arasu et al. [27] introduced a low-power and area-efficient FPGA design for two-dimensional DWT tested on CT, MRI, and fused images. This design incorporates 464 flip-flops, 4858 lookup tables, and 2774 slice blocks [27]. Recently, Bamerni et al. [16] proposed a fully integer-to-integer, memory-efficient, and parallel architecture for two-dimensional HWT using lifting scheme.

However, there could be a scope to enhance medical image quality through using wavelet based denoising with Ridgelet curvelet based hybrid edge detection and preservation techniques. Here an attention has been made to utilize the concept of modified HWT [10], modified Ridgelet, and curvelet based techniques to enhancement medical image. Further here in-place calculation has been used with lifting and sliding window protocol, which makes the proposed algorithm suitable for hardware implementation. The present work describes a novel idea for denoising as well as image enhancement using edge preservation and efficient hardware implementation. Most of the available methods in literature are based on software implementation. For real time performance of any system required hardware implementation. The hardware implementation of image enhancement algorithm is few.

The important offerings of the proposed work are as below-

In this research work, a modified HWT (MHWT) using lifting scheme has been used for denoising of medical images.

In the proposed method, the wavelet construction takes place in the predict step of the lifting scheme, which serves as a high-pass filter. In the update step, a scaling function is performed to produce a smoother version of images.

In the proposed method a cross-diagonal radon transform (modified Ridgelet) has been perform to get the edge information from high-pass image component.

Optimized resource utilization has been achieved by concept of pipelining. Further it has been implemented in tiny embedded system architecture to make it real time and portable solution.

The rest of the manuscript has been structured as follows. The proposed design methodology is described in Section- 2. The experimental results and analysis have been given with the fair comparisons and discussion in Section- 3. Finally, overall summary of the work has been concluded in Section- 4.

**The Proposed Methodology**

The proposed methodology has been discussed on the basis of experimental data set, development of the algorithm and dedicated embedded hardware system along with compact camera module in following subsections, as below.

Subject & Data Set Description

The summering of datasets used for this study has been shown in Table 1. The subjects include both male as well as female patients; categorized into two age groups, 18- 40 and above 40 years. Also, both sets include normal and abnormal cases diagnosed by expert medical practitioner form Department of Neuro-Surgery, R. G. Kar M.C. Hospital, Kolkata, India.

The patients in the abnormal set are suffering from mental disorders such as stroke, tumor, epileptic seizures, etc. The PET and CT imaging modalities are used as data for normal and abnormal patients. For one patient, we used 64 or 90 slices of 2D images. Each slice has dimension of 128x128 pixels for PET and 512x512 pixels for CT. Therefore, a particular subject has either 128(64 * 2 = 128) and/or 180(90 * 2 = 180) image slices. In the used dataset, a total of 14,000 image slices are present, consisting half of both PET and CT images. Further, the detailed of the datasets is shown in table 2.

**Table 1: Detail description of subject (Patient)**

| | Detail description of subject (Patient) | | | |
|---|---|---|---|---|
| SEX | Age Group (18 - 40 Year) | | Age Group (Above 40 Year) | |
| | Abnormal | Normal | Normal | Abnormal |
| M | 11 | 4 | 12 | 23 |
| F | 2 | 6 | 9 | 18 |

**Table 2: Detail description of image data set**

| Image Data Set Description | | | |
|---|---|---|---|
| Number of Subject | Slice per Subject | Image Type | Image Slice Dimension |
| 60 | 90 | PET | 128 x 128 |
| 25 | 64 | PET | 128 x 128 |
| 60 | 90 | CT | 512 x 512 |
| 25 | 64 | CT | 512 x 512 |

Algorithm Development

In this section a detailed discussion has been made on proposed algorithm in two parts. One is denoising and another is edge preservation. Below an algorithm design for image denoising based on non-separable modified Haar wavelet transform along with a modified Ridgelet, curvelet based edge preservation algorithm for medical images enhancement has been performs. Further it has been implemented into an embedded hardware platform to achieved portability and real time processing.

*Design of Denoising Algorithm*

In this part, the proposed algorithm design for image denoising based on non-separable modified Haar wavelet transform. It begins to perform wavelet transform as soon as getting the information of two pixels and stops just after processing the last pixel information. So, there is no need to wait for complete image at initial point of time. Further it can successfully perform 3rd level of denoised as soon as getting only four consecutive pixels information. Here in the proposed algorithm a modified version of the basic Haar wavelet transform is used along with lifting and in-place calculation with the help of sliding window techniques. Further the hardware implementation of the proposed algorithm can work with less deterioration even at high noise level. Here pipeline processing techniques has been used to achieve optimal hardware resource utilization and successfully reduced the algorithmic iteration. Also, in this method, as an alternative of a set of filters, a simple predict and update process of lifting scheme is used. The steps of the algorithm are in two stages- denoising and edge preservation, which are described in Algorithm 1 and Algorithm 2.

***Algorithm 1:*** *Denoising Based on MHWT*

**Input:** *Input images (PET, CT, MRI, etc.)*

**Output:** *Denoised images (PET, CT, MRI, etc.)*

Steps:

Start

Group all pixels into even and odd sets using the pixel index, $I_{Even}$ and $I_{Odd}$, where $I$ is a 1D image and n indicate the level of denoising. Therefore, $I_n$ can be defined as union of all even ($I_{Even}$) and odd ($I_{Odd}$) pixels at the nth level of denoising.

$$I_n = (I_{n(Even)} \cup I_{n(Odd)}) \tag{1}$$

Calculate the detailed coefficient ( $I_{(n,i)}^{Detail}$ ) of Haar wavelet in predict step of Lifting scheme by using in-place calculation (*'i'* indicate the pixel index and *n* is a stage of denoising). Here, the detailed coefficient ( $I_{(n,i)}^{Detail}$ ) of $i^{th}$ pixel at $n^{th}$ level of denoising can be defined as half of the difference of $I_{n,(i+1)}^{th}$ and $I_{n,(i)}^{th}$ pixels.

$$I_{(n,i)}^{Detail} = \left[ \frac{I_{n,i+1} - I_{n,i}}{2} \right] \tag{2}$$

Calculate the approximation part of Haar wavelet, in update step of Lifting scheme using in-place calculation. First we calculate the average of two consecutive pixels $I_{n,(i+1)}^{th}$ and $I_{n,(i)}^{th}$ and after that add half amount of detailed coefficient's ( $I_{(n,i)}^{Detail}$ *getting from equation. 2*) value with the average value.

$$I_{n,i} = \left[ \frac{I_{n,i+1} + I_{n,i}}{2} + \frac{I_{n,i+1} - I_{n,i}}{4} \right] \tag{3}$$

Follow step 3 and step 4 until last pixel get processed.

End

The diagram of the pixel level execution and overall line diagram of the above discussed algorithms have been shown in figure-1 and figure-2 respectively. In Figure 1, the two pixels of given input image has been indicated by odd and even indexed pixel and a split operation on those pixels have been performed in first step of lifting scheme. As shown in Figure 1, in predict step, subtract the odd pixel value from even pixel value has been perform (shown as high pass in Figure 1). Further, in update step, a half amount of the result of predicted step has been added with the result of the update step (shown as low pass in Figure 1). Here, in Figure 1, half amount of the detailed coefficient's value (shown as *(high pass/2)* in Figure 1) represents the high frequency component of the given image. It includes edge information with some noise.

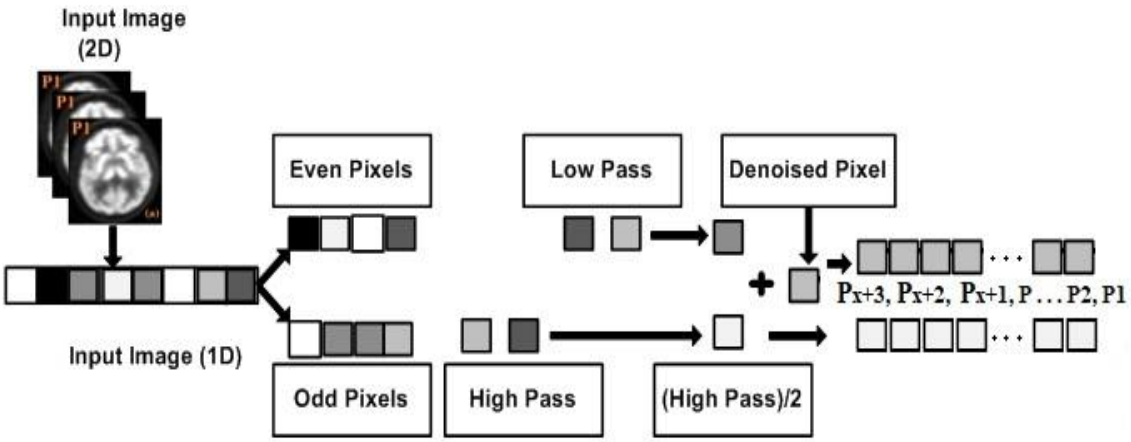


**Figure 1: Diagram of pixel level execution and output pixel generation**

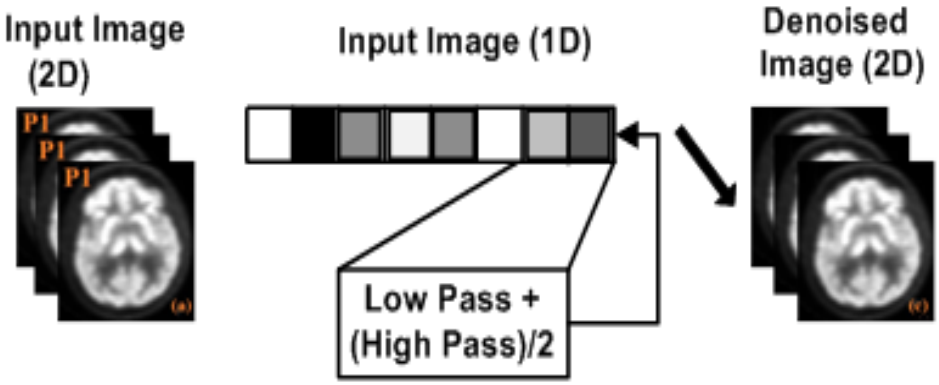


**Figure 2: Diagram of denoising part of the proposed algorithm**

The above steps also specify the adopted modification of the lifting scheme as well as basic HWT technique for this work. The diagram of overall execution and denoised output image generation of the said system is shown in Figure 2. In Figure 2 it has been shown that the 2D-image slices of the given 3D medical image have been further represented as 1D image. After that the proposed denoising operation has been performed on 1D image (PET, CT, MRI, etc.) respectively. After that, individually denoised image has been used as an input image of the edge preservation algorithm (Algorithm 2).

*Design of Edge Preservation Algorithm*

Here approximate digital implementations of two mathematical transforms- the Ridgelet transform [20] and the curvelet transform [21] have been done to achieve effective edge recovery while maintaining low computational complexity. A modification has been made to the original local Ridgelet transform (LRT) [28]. In this updated approach, we sum the values of both diagonal pixels and adjust the target pixel in a local box of four pixels, concentrating exclusively on the output component of the high-pass filter.

The Ridgelet transform employs a specialized over-complete wavelet pyramid on the radon transform, featuring wavelets that possess compact support in the spatial domain. The curvelet transform builds upon this Ridgelet transform as a foundational step, effectively implementing curvelet sub-bands and leveraging wavelet filters derived from the low-pass filter output obtained in Algorithm 1.

Furthermore, reconstructions utilizing the curvelet transform demonstrate superior perceptual quality compared to those based solely on wavelets, resulting in visually sharper images. This approach notably enhances the recovery of edges as well as subtle linear and curvilinear features. The existing theoretical framework surrounding the curvelet

and Ridgelet transforms indicates that these innovative methods can outperform wavelet techniques in specific image reconstruction contexts. The reported empirical results are promising and lend support to this theory [22].

***Modification on local Ridgelet transforms (LRT):***

The Ridgelet transform is particularly effective for detecting global lines that match the size of the image. To identify line segments, a partitioning method must be implemented [29]. The image can be divided into overlapping blocks, each with a side length of 'b' pixels. The overlap between vertically adjacent blocks forms a rectangular area of 'b' by "b/2", which helps to mitigate blocking artifacts. In an x by y image, we can identify "2n\b" blocks in each direction, leading to an increase in the redundancy factor by a factor of 4.

We calculate a pixel value, Pi from its four corresponding block values of half-size m = b/2, namely, *P1[c1, r1], P2[c1, r2], P3[c2, r1]* and *P4[c2, r2]* with *c1, r1 > b/2* and *c2 = c1 − m, r2 =r1 − m*, in the following way:

$$\left\{\begin{array}{l} f_1 = w\left(\frac{c_2}{m}\right)P_1[c_1, r_1] + w\left(1-\frac{c_2}{m}\right)P_4[c_2, r_2] \\ f_2 = w\left(\frac{c_2}{m}\right)P_2[c_2, r_1] + w\left(1-\frac{c_2}{m}\right)P_3[c_1, r_2] \\ P_i = w\left(\frac{r_2}{m}\right)f_1 + w\left(r-\frac{r_2}{m}\right)f_2 \end{array}\right\} \quad (4)$$

where $w(x) = \cos^2\left(\frac{\pi x}{2}\right)$ is the window. Of course, one might select any other smooth, non-increasing function satisfying, w(0) = 1, w(1) = 0, w′(0) = 0 and obeying the symmetry property w(x) + w(1 − x) = 1.

***Algorithm 2:*** *Edge Preservation*

**Input:** High & Low pass filter output getting from Algorithm 1

**Output:** Enhanced image

Steps:

Formed a local box of 2X2 pixels by using P1(c1,r1), P2(c1,r2), P3(c2,r1), and P4(c2,r2) pixels getting from high filter.

Perform modified local Ridgelet transforms by using the equation (4) on the above local box constricted from high pass filter's output. After that update the target pixel $\boldsymbol{P_{i\,(HPF)}}$, here 'i' represent the pixel index of the given image.

Now adding the value getting from step 2 with the value of same indexed pixel getting from low pass filter.

$$\boldsymbol{P_{i\,(HPF)} = P_{i\,(LPF)}, + P_{i\,(HPF)}} \quad (5)$$

Repeat Step 2 and Step 3 for all pixels of the given image.

Convert 1D image to 2D image.

End

An overall visualization of algorithm 1 and algorithm 2 has been shown in figure 3 below-

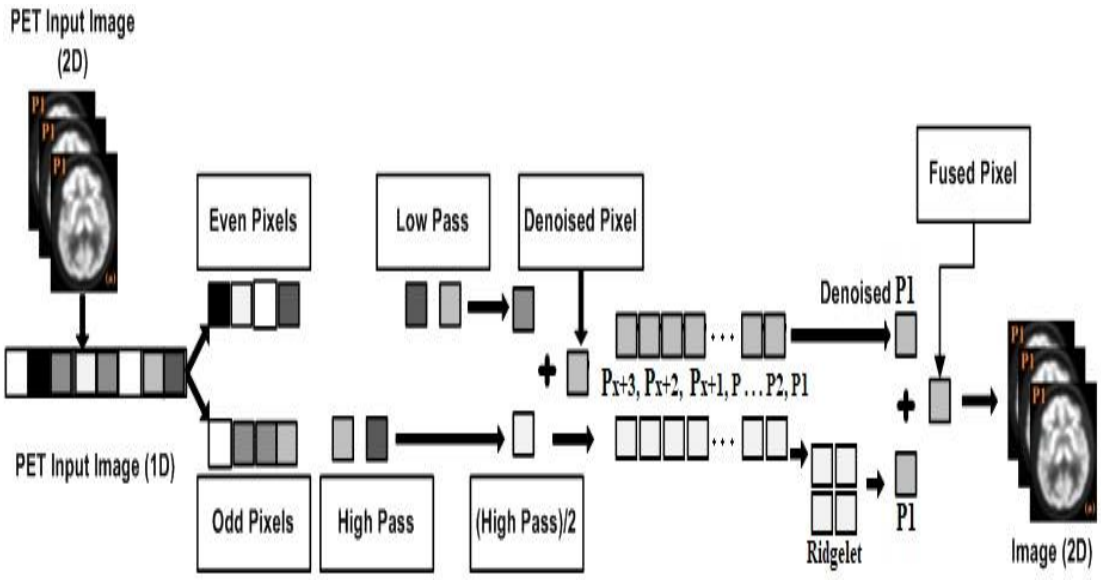


**Figure 3: Visualization of the proposed algorithm**

Hardware Efficient Embedded System Design

In the single cycle format, as depicted in Figure 4 (left side), the SD Card is used to store image data after completion of each level of denoising process. Initially, the input data (pixels) are retrieved from the SD card and transferred to the internal register memory. After obtaining the input image, the processor doing the necessary operations on these pixels and then saves the output pixel data back to the SD card. This process is then repeated for multiple pixels and multiple level of denoising.

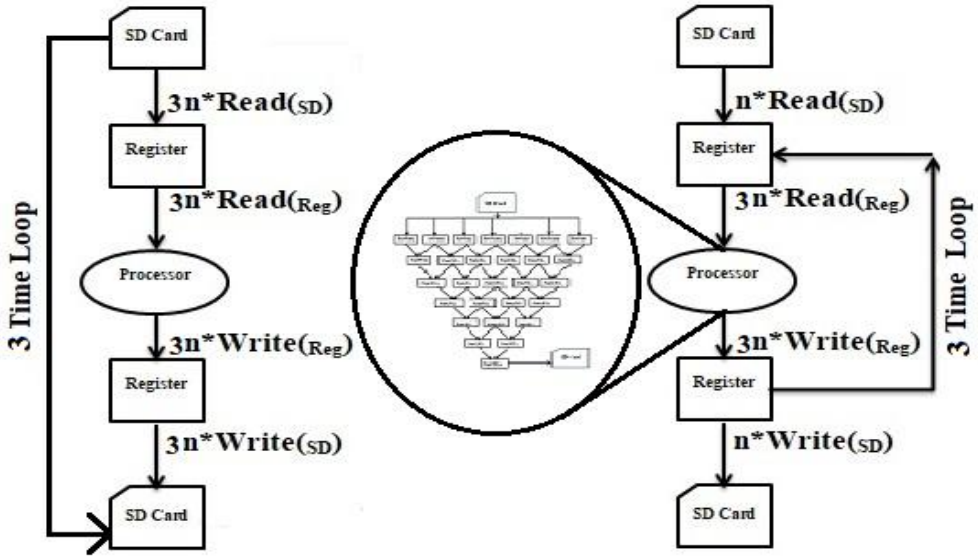


**Figure 4: Cyclic Execution of Proposed Algorithm with Optimization Read and Write Operation**

Figure 4 (right side) outlines a scheme for executing multiple pixels and multiple iteration of the proposed denoising algorithm. When considering x by y size image of n pixels (n=x*y), the processor requires “n” read operations from the SD Card to retrieve each pixel and “n” write operations to store the data back to the SD Card.

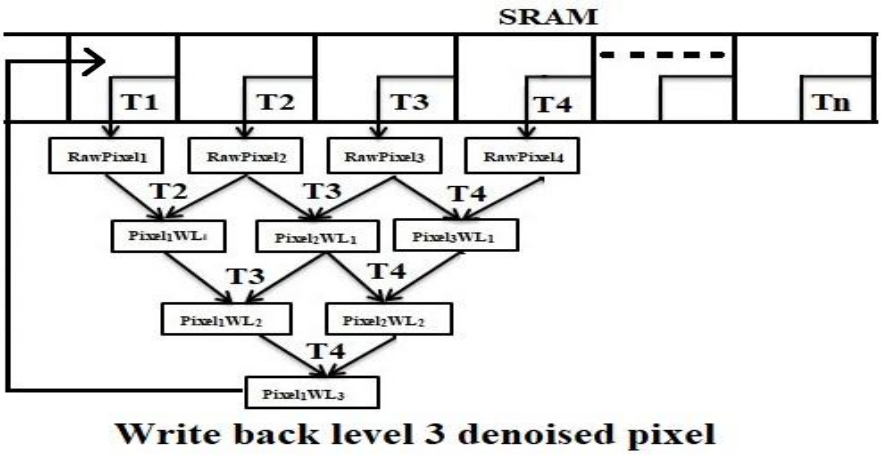


**Figure 5: Pipeline representation of 3rd level of denoising.**

Here the proposed algorithm performs the 3rd level of denoising required "*3*n*" times, SD Card and register read/write operations. So this process becomes time consuming due to the many read/write operations on SD cards. To address this issue, a software pipelining approach is used and implementation of software pipelining is described in Fig. 5 through a required resource and availability graph. If level 3 denoised single pixels are required, and then must have at least four pixels at a time. Fig. 5 shows that a level 3 denoised pixel is stored in register memory (image buffer register) and finally written to the SD card at once. This approach makes the proposed algorithm more efficient in terms of time complexity. Because the time requisite for fetching pixel value from an SD card and write the output pixel value to the SD card is much more than register read-write. In figure 6, a memory efficient implementation of algorithm 1 and algorithm 2 has been shown. Here, an image buffer of size *x+2* is used to store a window of n pixels. Where x denotes the number of columns of the input image and 'n' is a count up to second pixel of second row of that image. This approach provides all four required pixels for algorithm 1 and algorithm 2. From the algorithm 1 we get denoised pixels and high pass component of them which store separately for further use in algorithm 2. Perform edge preservation (Ridgelet operation) on the high pass component using pixels $P_1$, $P_2$, $P_{X+1}$, and $P_{X+2}$ and get the enhanced pixel '$P_1$'. Now sum up the enhanced $P_1$ with denoised pixel $P_1$ and get final enhanced pixel. In this greedy execution policy, there is no need to store whole input image at any point of time. Here in one go perform all three level of denoising and also preserved the edges. In this way the proposed algorithm achieved the space and time efficiency.

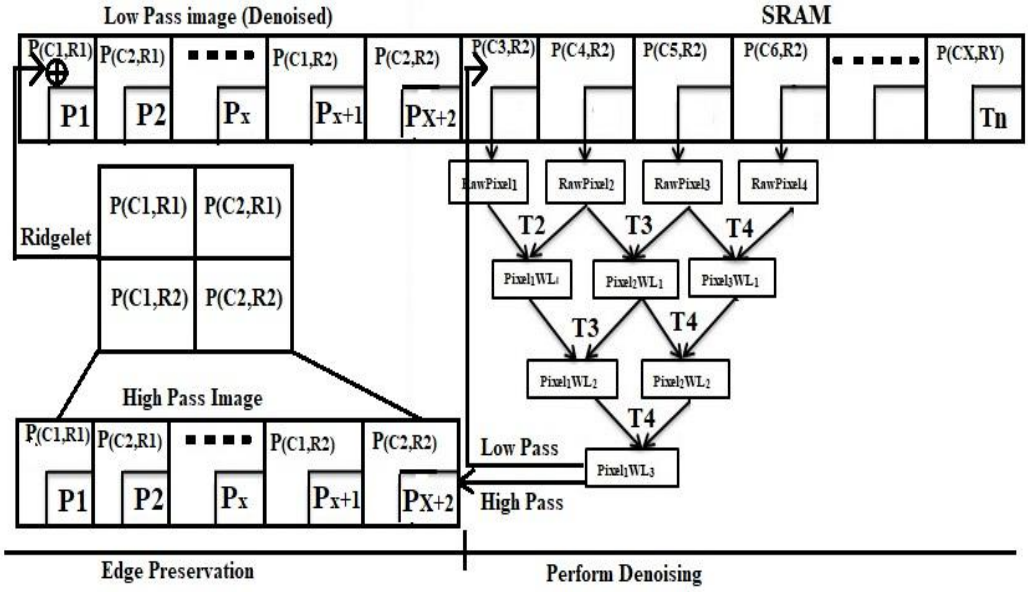


**Figure 6: Memory efficient execution of the proposed method.**

## 3. EXPERIMENTAL RESULTS

In this section, detailed description of the software as well as hardware output has been given and the results have been statistically analysed. Further, the work has been compared with available state-of-the-arts in different subsections as below-

Software and hardware output of given images (PET, CT, etc.)

This section presents the detailed analysis of pre and post denoising of PET and CT images. As per the dataset which we have used, each patient has either 128 or 180 PET and CT image slices. The dimensions of PET and CT images are 128x128 pixels and 512x512 pixels respectively. Figure 4 shows a 3D PET image of human brain using 90 slices. Here, the experiment involved a total of 85 patients, resulting in 14,000 image slices (7,000 both for PET and CT). For simplicity, the results of eight randomly selected slices have been shown for four patients, as representative case. These results are shown in Figure 7.

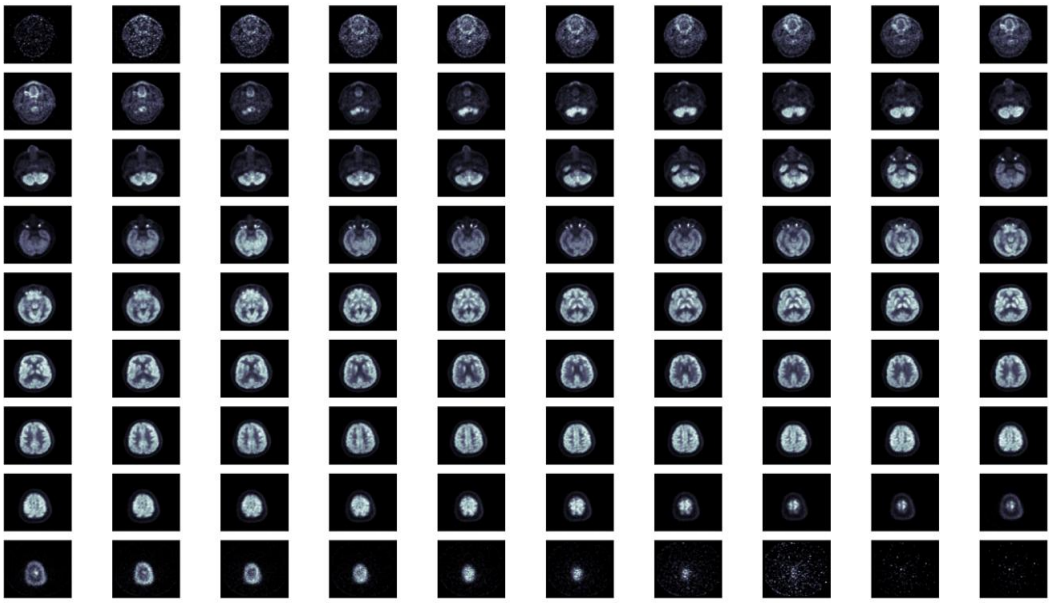

**Figure 7: Display a PET image data of single patient having 90, 2D slices with 128 x 128 dimensions.**

In Figure 8, PET, CT, and their corresponding outputs for four patients P1, P2, P3, and P4 have been shown. Figure 8(a) and 8(b) shows input PET and CT images of patient. Figure 8(c) and 8(d) show the corresponding denoised output images using the proposed method for PET and CT, respectively. The proposed technique was tested on PET and CT images of 85 patients. Further in figure 9 an enhanced output image of the proposed method has been shown. Here in figure 9 left one is a raw output image of the proposed algorithm, middle one is a color map image of the same left image, and right one is only Ridgelet part of the enhanced image.

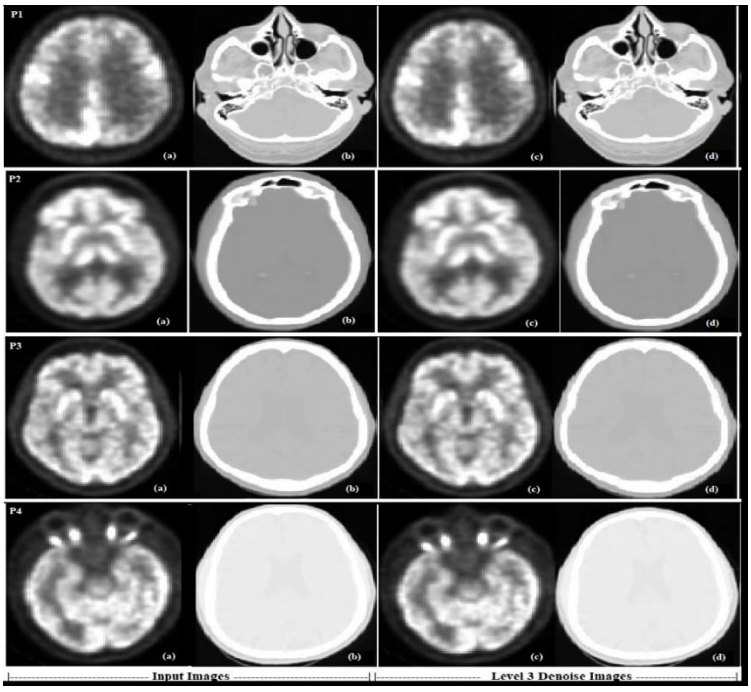


**Figure 8: The PET and CT images of four different patients (P1, P2, P3, and P4), pre and post denoising (a)-(b) input PET and CT images (c)-(d) corresponding denoised images using the proposed method.**

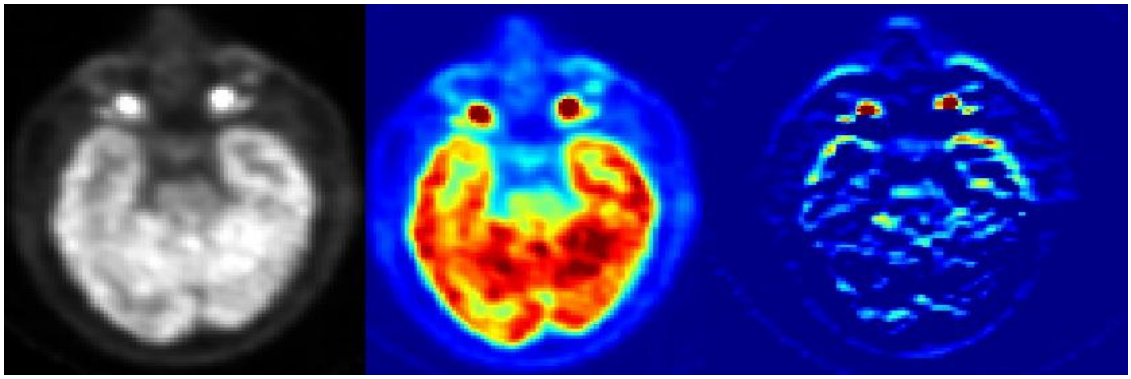

**Figure 9: Enhanced output of the proposed system (Left one is a raw output image of the proposed algorithm, middle one is a color map image of the same image, and right one is only Ridgelet part of the enhanced image).**

Statistical Analysis and Comparison

This section describes a detailed analysis of various performance metrics required to assess the image quality. Also, for fair comparison, the proposed hardware design has also been compared and contrasted with recent state-of-the-arts available in literature.

*Image Quality Measurement Statistics*

*Mean Square Error (MSE) and Peak Signal to Noise Ratio (PSNR):* MSE and PSNR are used to measure the quality of denoised image. MSE is the cumulative squared error between denoised and original image, whereas PSNR is a measure of the peak error. MSE and PSNR are defined as below [28-30].

$$MSE = \left( \frac{1}{MN} \sum_{j=1}^{M} \sum_{i=1}^{N} \left[ x(i,j) - y(i,j) \right]^2 \right) \tag{6}$$

$$PSNR = 20 * \log_{10}\left(\frac{255}{\sqrt{MSE}}\right) \tag{7}$$

where x is the original image, y is the denoised image, and ($M * N$) is the dimension of the images. The lower value for MSE indicates better denoised image, and a high value of PSNR corresponds to good image quality [28-30].

***Universal Image Quality Index (UIQI):*** It indicates the image quality distortion. For two images x and y, the UIQI is calculated as a product of three components:

$$Q = \left(\frac{\sigma_{xy}}{\sigma_x \sigma_y} * \frac{2x'y'}{(x')^2 + (y')^2} * \frac{2\sigma_x \sigma_y}{\sigma_x{}^2 + \sigma_y{}^2}\right) \tag{8}$$

where the first, second and third components indicate the correlation coefficient between x and y, the similarity among the mean luminance x and y, and the similarity in contrast of the two images respectively [29-31].

***Mutual Information (MI):*** It measure the amount of information that a fused image, F contains about x and y. [30-32].

$$F(x,y) = \sum_{x,y}\left(P_{(x,y)} \log\left(\frac{P_{(x,y)}}{P_{(x)}P_{(y)}}\right)\right) \tag{9}$$

$$I_{F,X}(f,x) = \sum_{a,b} P_{FX}(f,x) \log\left(\frac{P_{FX}(f,x)}{P_F(f)P_X(x)}\right) \tag{10}$$

$$I_{F,X}(f,y) = \sum_{a,b} P_{FY}(f,y) \log\left(\frac{P_{FY}(f,y)}{P_F(f)P_Y(y)}\right) \tag{11}$$

Thus, the Mutual Information is given by

$$M_F^{XY} = I_{FX}(f,x) + I_{FY}(f,y) \tag{12}$$

***Geometric Mean (Gm):*** The arithmetic mean is what people are usually talking about when they say "average". By far the most widely used, it's simple to calculate: you sum the parts, then divide by how many there were. The geometric mean has the same procedure but different operations. You multiply the parts, then take the root corresponding to how many there were. The geometric mean is often used when finding the mean of data which are measured in different units [33].

***Gradient (Gd):*** To calculate the gradient of any line, the x and y coordinates of a line are used. In other words, it is the ratio of the change in the y-axis to the change in the x-axis. The formula to calculate the gradient of a line is given as, where m represents the gradient of the line [34].

$$m = \frac{(y_2 - y_1)}{(x_2 - x_1)}$$
$$m = \frac{\Delta y}{\Delta x} \tag{15}$$

To assess the output image quality, in absence of ground truth, variable noise addition technique has been used [35]. For one representative experiment, *"Poisson"* noise with a standard deviation 0.05 and offset 0.01 has been added to the primary image. Further, denoising operation has been performed up to third level of decomposition, as

denoising results obtained up to third level are clinically acceptable by medical practioners. For the performance evaluation of the proposed MHWT method, the results have been compared with the traditional DWT based method, in terms of different quantitative measures (PSNR, MSE, and UIQI) as shown in table 3.

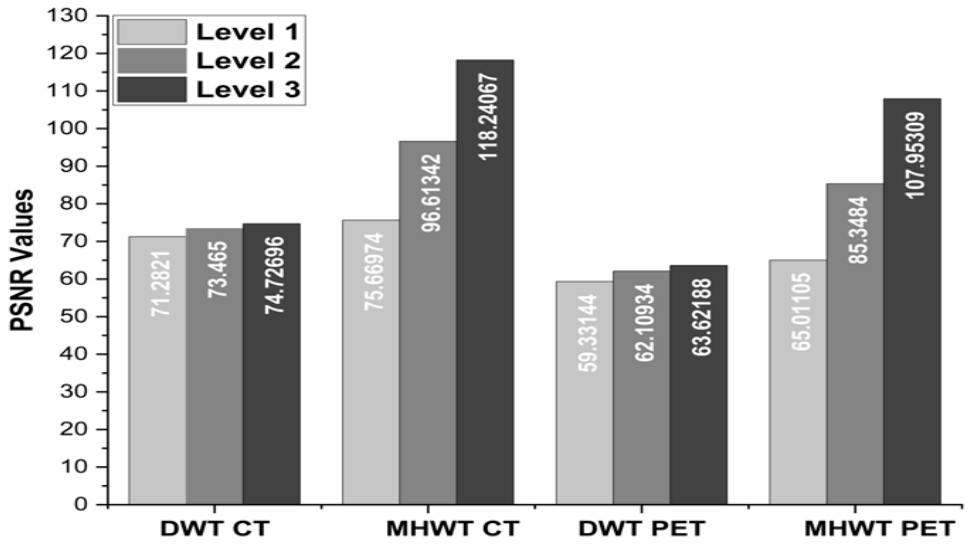


**Figure 10(a): PSNR Graph: The level-wise average of PSNR values of DWT2 algorithm and the proposed MHWT algorithm.**

Level-wise averages of PSNR values have been presented in table 3 for both DWT2 and MHWT algorithms and shown in figure 10(a). It is clear from the figure that PSNR values obtained by the proposed MHWT algorithm are better as compared to DWT2 algorithm. From figure 10(a), it has also been observed that the level-wise performance of the MHWT algorithm is better than DWT2 based algorithms. This is due to the modification in denoising process in case of NS-HWT algorithm. By this proposed method, the noise from the given image has been successfully removed due to the modification at high-pass filter level.

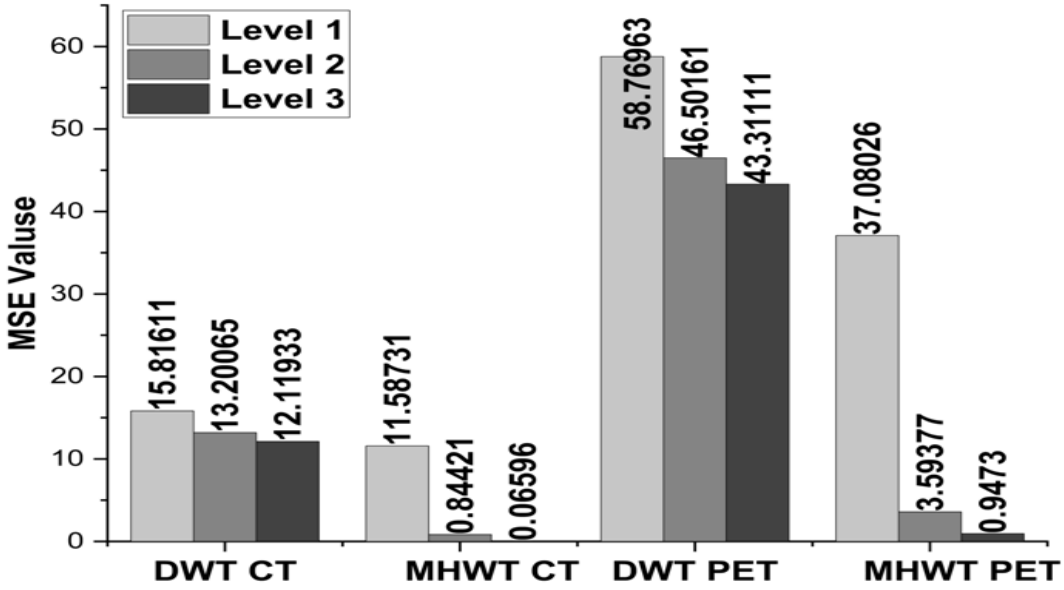


**Figure 10(b): MSE Graph: The level-wise average of MSE values of DWT2 algorithm and the proposed MHWT algorithm.**

For MSE, again level-wise average of MSE values has been calculated from table 3 for the studied algorithms and shown in figure 10(b). It has been observed from the figure that the MHWT algorithm exhibits significant decrease

in mean square error as compared to DWT2 based algorithms due to the increase in accurate prediction of image pixels during denoising.

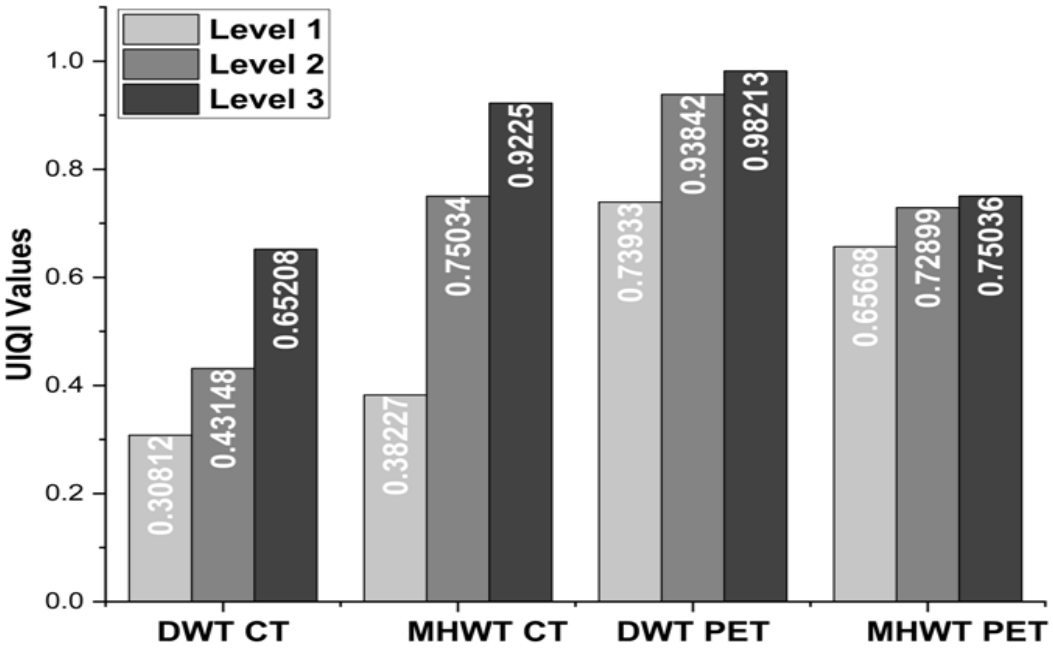


**Figure 10(c): UIQI Graph: The level-wise average of UIQI values of DWT2 algorithm and the proposed MHWT algorithm.**

The average UIQI values of the studied algorithms for CT and PET images have been shown in figure 6(c). Here, MHWT method results in better UIQI values for CT images and a comparable performance with DWT2 algorithm for PET images.

**Table 3: Values of MSE, PSNR, and UIQI of denoised PET and CT Images**

| **Patient 1** | | | | | | | |
|---|---|---|---|---|---|---|---|
| **Algorithm** | **Images** | CT-Image | | | PET-Image | | |
| | | **MSE** | **PSNR (dB)** | **UIQI** | **MSE** | **PSNR (dB)** | **UIQI** |
| **DWT2** | Input Image | 68108.84842 | +0.33447 | 0.24657 | 537114.17169 | +18.27173 | 0.49115 |
| | Level 1 | 14.84521 | +72.89787 | 0.38655 | 50.08105 | +62.33613 | 0.76160 |
| | Level 2 | 13.12524 | +73.96745 | 0.40996 | 46.19531 | +63.03764 | 0.95319 |
| | Level 3 | 12.57570 | +74.33896 | 0.65841 | 43.96118 | +63.46821 | 0.99300 |
| **Proposed MHWT** | Input Image | 68108.84842 | +0.33447 | 0.24657 | 537114.17169 | +18.27173 | 0.49115 |
| | Level 1 | 10.92262 | +75.56307 | 0.34129 | 42.33423 | +63.79577 | 0.69068 |
| | Level 2 | 0.87052 | +97.53401 | 0.80136 | 3.88770 | +84.53575 | 0.74180 |
| | Level 3 | 0.07698 | +118.60197 | 0.91995 | 0.29688 | +106.87813 | 0.75694 |
| **Patient 2** | | | | | | | |
| **Algorithm** | **Images** | CT-Image | | | PET-Image | | |

| | | **MSE** | **PSNR (dB)** | **UIQI** | **MSE** | **PSNR (dB)** | **UIQI** |
|---|---|---|---|---|---|---|---|
| **DWT2** | Input Image | 71598.58635 | +0.76849 | 0.23655 | 202780.91772 | +9.81094 | 0.49869 |
| | Level 1 | 15.23706 | +72.67157 | 0.37083 | 64.67578 | +60.11476 | 0.75050 |
| | Level 2 | 12.72437 | +74.23688 | 0.39101 | 47.58691 | +62.77985 | 0.94070 |
| | Level 3 | 12.57246 | +74.34119 | 0.63612 | 43.79785 | +63.50054 | 0.98659 |
| **Proposed MHWT** | Input Image | 71598.58635 | +0.76849 | 0.23655 | 202780.91772 | +9.81094 | 0.49869 |
| | Level 1 | 10.71794 | +75.72737 | 0.36938 | 29.08185 | +67.05716 | 0.67821 |
| | Level 2 | 0.88059 | +97.43410 | 0.79993 | 2.62781 | +87.93773 | 0.73512 |
| | Level 3 | 0.07565 | +118.75394 | 0.92358 | 0.24139 | +108.67507 | 0.75090 |
| **Patient 3** | | | | | | | |
| **Algorithm** | **Images** | CT-Image | | | PET-Image | | |
| | | **MSE** | **PSNR (dB)** | **UIQI** | **MSE** | **PSNR (dB)** | **UIQI** |
| **DWT2** | Input Image | 65408.14002 | +0.44347 | 0.42055 | 548114.16971 | +15.04812 | 0.50845 |
| | Level 1 | 14.94509 | +71.10787 | 0.24052 | 52.08325 | +60.21610 | 0.66105 |
| | Level 2 | 13.52022 | +72.96745 | 0.42990 | 47.09551 | +62.03004 | 0.92329 |
| | Level 3 | 12.07170 | +74.83290 | 0.68048 | 42.96058 | +64.46128 | 0.98305 |
| **Proposed MHWT** | Input Image | 65408.14002 | +0.44347 | 0.42055 | 548114.16971 | +15.04812 | 0.50845 |
| | Level 1 | 11.96282 | +74.66370 | 0.33128 | 48.38012 | +64.02554 | 0.68260 |
| | Level 2 | 0.97087 | +96.58801 | 0.70163 | 4.80470 | +82.03537 | 0.74694 |
| | Level 3 | 0.05635 | +118.08194 | 0.91588 | 0.19606 | +107.05413 | 0.76145 |
| **Patient 4** | | | | | | | |
| **Algorithm** | **Images** | **CT-Image** | | | **PET-Image** | | |
| | | **MSE** | **PSNR (dB)** | **UIQI** | **MSE** | **PSNR (dB)** | **UIQI** |
| **DWT2** | Input Image | 70278.53685 | +0.84689 | 0.37083 | 202646.73016 | +9.81094 | 0.49869 |
| | Level 1 | 18.23706 | +68.45107 | 0.23456 | 68.23845 | +54.65875 | 0.78415 |
| | Level 2 | 13.43277 | +72. 68823 | 0.49504 | 45.12870 | +60.58981 | 0.93648 |
| | Level 3 | 11.25746 | +75.39479 | 0.62582 | 42.52483 | +63.05748 | 0.96589 |
| **Proposed MHWT** | Input Image | 70278.53685 | +0.84689 | 0.36938 | 202646.73016 | +9.80519 | 0.49923 |
| | Level 1 | 12.74514 | +76.72481 | 0.48712 | 28.52483 | +65.16574 | 0.57521 |
| | Level 2 | 0.65487 | +94.89754 | 0.69845 | 3.05487 | +86. 88473 | 0.69209 |
| | Level 3 | 0.05487 | +117.52481 | 0.93058 | 0.08547 | +109.20504 | 0.73215 |

In table 3 and 4, a list of statistical parameters has been calculated of the proposed algorithm to establish the quality of enhanced output images. Same time a comparison with basic version of the algorithm is provided. Table 3 show denoised part of proposed algorithm provide very good denoised image as intermediate output of the algorithm. The output image (pixels) is used as an input to edge enhancement part of the proposed algorithm and produced the final output image. Here table 4 shows that output image quality with the help of some statistical parameters namely MSE, PSNR, Gm, and Gd. Further low MSE value and high PSNR value of our proposed algorithm comparison with the basis version of the curvelet algorithm, confirmed that the quality of output image is good. Furthermore, by the level wise low MSE and high PSNR value of our proposed algorithm confirm that the quality of the output image in increasing level by level. Other side, on the basis of Gm and Gd we can conclude that, the enhanced image have good amount of edge and curve information. These edge and curve information have been added with the denoised image and enhanced the quality of the image.

Thus, it is clear from above discussions that the performance of the proposed algorithm is better as compared to available basic curvelet and Ridgelet based algorithm. Further, a hardware-level comparison has also been presented in next subsection.

**Table 4: MSE, PSNR, Gm, and Gd Values of Enhanced Images**

| Image enhancement using basic curvelet techniques (PET Image) | | | | |
|---|---|---|---|---|
| **Image** | **MSE** | **PSNR dB** | **Gm** | **Gd** |
| **Input** | 537080.7836 | 0.27119 | 68.14231 | 79.23990 |
| **L1** | 92694.47394 | 3.01148 | 15.41553 | 70.85224 |
| **L2** | 93.4986 | 56.9135 | 1.98772 | 21.39210 |
| **L3** | 6.9364 | 79.50691 | 0.29871 | 6.08272 |
| Image enhancement using proposed algorithm (PET Image) | | | | |
| **Image** | **MSE** | **PSNR dB** | **Gm** | **Gd** |
| **Input** | 537080.7836 | 0.27119 | 68.14231 | 79.23990 |
| **L1** | 6122.64246 | 20.59082 | 52.75579 | 76.91531 |
| **L2** | 5.11383 | 82.15467 | 6.81606 | 39.86131 |
| **L3** | 0.44342 | 103.39329 | 1.32904 | 24.43565 |

*Hardware Level Comparison*

The proposed algorithm has been implemented using MATLAB (R2015b, 64-bit). The testing involved PET, and CT images of size *128x128*, 256x256, and *512x512* pixels, respectively. Table 5 represents a hardware level comparison of the proposed image enhancement algorithm on the basis of resource utilization. It is presented a comparison with state-of-the-art methods based on their memory usage, CPU requirements, and dependency on a GPU. Each method is accompanied by its respective memory usage (in MB), whether it necessitates a 64-bit CPU, and its reliance on a GPU for operation. Notably, the proposed method distinguishes itself with remarkably low memory usage (0.004MB), a 32-bit CPU requirement, and independence from a GPU. This analysis provides valuable insights into the resource demands of different methods for specific applications. The attributes of the proposed embedded system render it an exceptionally lightweight and cost-effective solution, well-suited for real-time edge processing systems.

**Table 5: Comparison with various state-of-the-art methods**

| **Methods** | **Memory Requirement (MB)** | **Required CPU** | **Required GPU** |
|---|---|---|---|
| VessNetar [36] | 36.600MB | 64-bit | Yes |
| MobileNet-V3 [37] | 11.000MB | 64-bit | Yes |
| RSFNet [38] | 8.000MB | 64-bit | Yes |

| | | | |
|---|---|---|---|
| PLVSNet [39] | 3.600MB | - | - |
| M2UNet [40] | 2.200MB | 64-bit | Yes |
| G-Net Light [41] | 1.520MB | 64-bit | Yes |
| LDMRes-Net [42] | 0.580MB | - | - |
| **Proposed Method** | **0.004MB** | **32-bit** | **No** |

## 4. CONCLUSION

In this work, an embedded hardware implementation using modified HWT, curvelet, and modified Ridgelet based image enhancement algorithm has been proposed and studied on PET and CT brain images. The proposed technique successfully eliminates high levels of noise, preserved the edge and curve information of the same input image at a time which enhanced the quality of input image. This has been verified with the performance evaluation of various image quality assessment parameters. Furthermore, hardware implementation of the proposed algorithm signifies the utilization of only 0.004MB memory. This it confirms the successful attainment of hardware advantages in terms of area. In continuation for fair comparison, embedded implementation of the proposed algorithm has been compared and contrasted with the available state-of-the-arts. By means of experimentations, it has been proved that the proposed method suggests much faster, portable, and cost-effective hardware architecture than others. In future, the proposed method could also be extended for FPGA implementation using new generation wavelet, curvelet and Ridgelet based techniques for better quality of output images.

**Acknowledgment:**

Authors would like to acknowledge Dr. Dinesh Jaluka, Associate Professor at Department of Neurosurgery, R. G. Kar medical college and hospital, Kolkata, India, for his suggestions as a field expert.

**Conflict of interest:** The authors have no conflict of interests.

**References:**

1. J. J. Huang and P. L. Dragotti, "WINNet: Wavelet inspired invertible network for image denoising," IEEE Transactions on Image Processing, vol. 31, pp. 4377–4392, 2022.
2. K. Mishiba, "Fast guided median filter," IEEE Transactions on Image Processing, vol. 32, pp. 737–749, 2023.
3. P. Pal and S. Singh, "Contrast enhancement of medical images: A review," IJRDO-Journal of Health Sciences and Nursing, vol. 1, no. 4, pp, 32 –35, 2016.
4. K. Das, D. Khorat and S. K. Sharma, "An embedded system for gray matter segmentation of pet-image," In Proceedings of the Global AI Congress 2019, vol. 1112, Springer Singapore, 2020, pp. 145–157.
5. A.S. Thokec, K. Vermaa and B. K. Singh, "An enhancement in adaptive median filter for edge preservation," Procedia Computer Science, vol. 48, pp. 29 – 36, 2015.
6. S. S. Bedi and J. Agarwal, "Implementation of hybrid image fusion technique for feature enhancement in medical diagnosis," Human-centric Computing and Information Sciences, vol. 3, no. 5, pp. 1–17, 2015.
7. F. Ghante, L. Tawade and A. B. Aboobacker, "Image fusion based on wavelet transforms," International Journal of Bio-Science and Bio-Technology, vol. 6, no. 3, pp. 149–162, 2014.
8. W. Tang, F. He, Y. Liu and Y. Duan, "MATR: Multimodal medical image fusion via multiscale adaptive transformer," IEEE Transactions on Image Processing, vol. 31, pp. 5134–5149, 2022.
9. S.G Mallat "A theory for multiresolution signal decomposition: the wavelet representation," IEEE Transactions on Pattern Analysis and Machine Intelligence, vol. 11, no. 7, pp. 674–693, 1989.
10. K. Das, M. Maitra, P. Sharma and M. Banerjee, "Early started hybrid denoising technique for medical images," In Recent Trends in Signal and Image Processing, vol. 727, Springer, 2019, pp. 131–140.
11. A. Bultheel, "Adaptive wavelet thresholding for image denoising and compression," IEEE Transactions on Image Processing, vol. 9, no. 9, pp.1532–1546, 2000.
12. W. Sweldens, "The lifting scheme: A construction of second generation wavelets." SIAM Journal on Mathematical Analysis, vol. 29, no. 2, pp. 511–546, Mar 1998.
13. W. Daubechies and I. Sweldens, "Factoring wavelet transforms into lifting steps," The Journal of Fourier Analysis and Applications, vol. 4, no. 3, pp. 247 – 269, 1998.
14. K. Das, M. Maitra, M. Banerjee and P. Sharma, "Embedded implementation of early started hybrid denoising technique for medical images with optimized loop," In Emerging Technology in Modelling and Graphics, vol. 937, Springer Singapore, 2019, pp. 295–308.
15. A. Balodi, R. S. Anand, M. L. Dewal and A. Rawat, "Severity Analysis of Mitral Regurgitation Using Discrete Wavelet Transform," IETE Journal of Research, vol. 69, no. 1, pp. 209-219, Sep. 2020.

16. S. A. Bamerni and A. K. Al-Sulaifanie, “An efficient non-separable architecture for haar wavelet transform with lifting structure,” Microprocessors and Microsystems, vol. 71, pp. 102881, 2019.
17. S. Sarkar and S. S. Bhairannawar, “Efficient FPGA architecture of optimized haar wavelet transform for image and video processing applications,” Multidimensional Systems and Signal Processing, vol. 32, no. 2, pp. 821–844, 2021.
18. O. S. Ojo, A. Chigozirim and O. D. Olu, “Implementation of wavelet-based architecture for optimization image filtering,” Information Technology Journal, vol. 19(1), pp. 1–11, 2020.
19. Bhadauria, H. S., & Dewal, M. L. (2012). Efficient Denoising Technique for CT images to Enhance Brain Hemorrhage Segmentation. Journal of Digital Imaging, 25(6), 782–791. https://doi.org/10.1007/s10278-012-9453-y
20. Candès, E. J. (1999). Harmonic analysis of neural networks. Applied and Computational Harmonic Analysis, 6(2), 197–218. https://doi.org/10.1006/acha.1998.0248
21. Olson, T., & DeStefano, J. (1994). Wavelet localization of the Radon transform. IEEE Transactions on Signal Processing, 42(8), 2055–2067. https://doi.org/10.1109/78.301841
22. Starck, N. J., Candes, E., & Donoho, D. (2002). The curvelet transform for image denoising. IEEE Transactions on Image Processing, 11(6), 670–684. https://doi.org/10.1109/tip.2002.1014998
23. A. Sangiovanni-Vincentelli, R. Murgai and R. K. Brayton, Logic Synthesis for Field-Programmable Gate Arrays, Springer US, 1995.
24. N. Sudha, C. S. S. Prasanna and V. Kamakoti, “An Efficient Digital Architecture for Principal Component Neural Network and its FPGA Implementation,” IETE Journal of Research, Vol. 53, no. 5, pp. 425-431, Oct 2007.
25. Y. Ding and J. Cong, “Combinational logic synthesis for LUT based field programmable gate arrays,” ACM Transactions on Design Automation of Electronic Systems, vol. 1, no. 2, pp. 145–204, 1996.
26. T. Lindblad and J. Chilo, “Hardware implementation of 1D wavelet transform on an FPGA for infrasound signal classification,” IEEE Transactions on Nuclear Science, vol. 55, no. 1, pp. 9 – 13, 2008.
27. S. Baulkani and S. P. V. Arasu, “An Efficient FPGA architecture with high-performance 2D DWT processor for medical imaging,” Journal of Circuits Systems and Computers, vol. 25, no. 9, pp. 1 – 22, 2016.
28. Fadili, J., & Starck, J. (2009). Curvelets and ridgelets. In Springer eBooks (pp. 1718–1738). https://doi.org/10.1007/978-0-387-30440-3_111
29. Candes, E. J., Donoho, D. L., Johnstone, I. M., & Papanicolaou, G. C. (2000). RIDGELETS: THEORY AND APPLICATIONS. https://candes.su.domains/publications/downloads/Thesis.pdf
30. Q. Huynh-Thu and M. Ghanbari, “Scope of validity of PSNR in image/video quality assessment,” Electronics Letters, vol. 44, no. 13, pp. 800 – 801, 2008.
31. Z. Wang and A. C. Bovik, “A universal image quality index,” IEEE Signal Processing Letters, vol. 9, no. 3, pp. 81– 84, 2002.
32. J. P. W. Pluim, J. B. A. Maintz and M. A. Viergever, “Mutual-information-based registration of medical images: a survey,” IEEE Transactions on Medical Imaging, vol. 22, no. 8, pp. 986 – 1004, 2003.
33. L. Persola, (2022, November 27). Visualizing the geometric and harmonic means - the startup - medium. Medium. https://medium.com/swlh/visualizing-the-geometric-and-harmonic-means-e8b9c5a818ae
34. Gradient of a line - formula, definition, examples. (last accessed: oct-2024). Cuemath. https://www.cuemath.com/geometry/gradient-of-a-line/
35. K. Dabov, A. Foi, V. Katkovnik and K. Egiazarian. Image denoising by sparse 3-d transform-domain collaborative filtering. IEEE Transactions on Image Processing, vol. 16, no. 8, pp. 2080–2095, Aug 2007.
36. M. Arsalan, M. Owais, T. Mahmood, S.W. Cho, and K.R. Park. Aiding the diagnosis of diabetic and hypertensive retinopathy using Artificial Intelligence-Based Semantic Segmentation. Journal of Clinical Medicine, 8(9):1446, 9 2019. doi: 10.3390/jcm8091446.
37. A. Howard, M. Sandler, G. Chu, L. C. Chen, B. Chen, M. Tan, W. Wang, Y. Zhu, R. Pang, V. Vasudevan, Q. V. Le, and H. Adam. Searching for MobileNetV3. arXiv (Cornell University), 1 2019. doi: 10.48550/arxiv.1905.02244.
38. E. Romera, J. M. Alvarez, L. M. Bergasa, and R. Arroyo. ERFNET: Efficient Residual Factorized ConVNet for Real-Time Semantic segmentation. IEEE Transactions on Intelligent Transportation Systems, 19(1):263–272, 10 2017. doi: 10.1109/tits.2017.2750080.
39. M. Arsalan, T. M. Khan, S. S. Naqvi, M. Nawaz, and I. Razzak. Prompt Deep Light-Weight Vessel Segmentation Network (PLVS-NeT). IEEE/ACM Transactions on Computational Biology and Bioinformatics, 20(2):1363-1371, 3 2023. doi: 10.1109/tcbb.2022.3211936.
40. T. Laibacher, T. Weyde, and S. Jalali. M2U-NET: Effective and efficient retinal vessel segmentation for Resource-Constrained environments. arXiv (Cornell University), 1 2018. doi: 10.48550/arxiv.1811.07738.
41. S. Iqbal, S. S. Naqvi, H. A. Khan, A. Saadat, and T. M. Khan. G-Net Light: a lightweight modified Google Net for retinal vessel segmentation. Photonics, 9(12):923, 11 2022. doi: 10.3390/photonics9120923.
42. S. Iqbal, T. M. Khan, M. Alhussein, S. S. Naqvi, M. Usman, and K. Aurangzeb. LDMRES-NET: Enabling efficient medical image segmentation on IoT and edge platforms. arXiv (Cornell University), 1 2023. doi:10.48550/arxiv.2306.06145..